is due to the combination of shorter bonds and reduced areal density, whereas the comparable compressibilities result from cancellation between different bonds per area and bond strengths. A direct test of this proposal can be performed if these experiments are extended to higher pressure; if the C_{60} bonds are indeed stiffer than in graphite, the compressibility should decrease rapidly with increasing P.

Isothermal volume compressibilities $-1/V(dV/dP)$ are 6.9×10^{-12}, 2.7×10^{-12}, and 0.18×10^{-12} cm^2/dyne for solid C_{60}, graphite, and diamond, respectively. Clearly, fullerite is the softest all-C solid currently known. The linear compressibility normal to the close-packed planes is nearly equal for solid C_{60} and graphite (11). This suggests that there should be no elastic impediments to the formation of "intercalated" (12) fullerites.

REFERENCES AND NOTES

1. W. Kratschmer, L. D. Lamb, K. Fostiropoulos, D. R. Huffman, Nature 347, 354 (1990).
2. R. M. Fleming et al., Mater. Res. Soc. Symp. Proc., in press.
3. H. Kroto, Science 242, 1139 (1988).
4. C. S. Yannoni, R. D. Johnson, G. Meijer, D. S. Bethune, J. R. Salem, J. Phys. Chem. 95, 9 (1991).
5. R. Tycko et al., ibid., p. 518.
6. H. Ajie et al., ibid. 94, 8630 (1990).
7. J. M. Hawkins et al., J. Org. Chem. 55, 6250 (1990).
8. P. A. Heiney et al., in preparation.
9. R. Clarke and C. Uher, Adv. Phys. 33, 469 (1984).
10. Manufactured by INEL, Les Ulis, France.
11. The effect of hydrostatic pressure on a cubic crystal is to reduce all lengths proportionally regardless of direction with respect to the crystal axes. Our results therefore show that the compressibility of close-packed (111) planes in cubic C_{60} is the same as that of the honeycomb (002) planes in hexagonal graphite.
12. J. E. Fischer and T. E. Thompson, Phys. Today 31 (no. 7), 36 (1978).
13. We acknowledge the technical assistance of O. Zhou and V. B. Cajipe. We are grateful to R. M. Fleming and E. J. Mele for helpful discussions and to F. A. Davis for the use of his HPLC column. This work was supported under National Science Foundation Materials Research Laboratory Program grant DMR88-19885 and under Department of Energy grants DE-FC02-86ER45254 and DE-FG05-90ER75596.

18 March 1991; accepted 18 April 1991

A Neuron-Silicon Junction: A Retzius Cell of the Leech on an Insulated-Gate Field-Effect Transistor

PETER FROMHERZ,* ANDREAS OFFENHÄUSSER, THOMAS VETTER, JÜRGEN WEIS

An identified neuron of the leech, a Retzius cell, has been attached to the open gate of a p-channel field-effect transistor. Action potentials, spontaneous or stimulated, modulate directly the source-drain current in silicon. The electronic signals match the shape of the action potential. The average voltage on the gate was up to 25 percent of the intracellular voltage change. Occasionally weak signals that resemble the first derivative of the action potential were observed. The junctions can be described by a model that includes capacitive coupling of the plasma membrane and the gate oxide and that accounts for variable resistance of the seal.

MULTISITE RECORDING OF THE electrical activity of neurons is a prerequisite to the study of signal processing in arborized neurons and in neural nets. Such a method must be noninvasive and should detect changes in intracellular voltage at a high spatial and temporal resolution. Optical recording by voltage-sensitive dyes (1, 2) and electrical recording by extracellular metallic electrodes on glass (3–6) or Si (7, 8) have been used. We report on a direct coupling of neural excitation and electrical current in Si in a transistor-type device. The assembly is a first step toward multiple recording in neurons and neural nets and toward the development of neural biosensors and neuroelectronic circuits.

A neuron is mounted on a thin insulating layer of a gate oxide on n-type Si in an electrolyte (Fig. 1). A positive-bias voltage is applied to the bulk Si to provide an accumulation of mobile, positive defect electrons near the surface (strong inversion). The positive voltage change in the neuron during an action potential lifts the surface potential of Si and reduces the density of mobile defect electrons. The neuron-Si interaction causes a modulation of the current along the inversion layer (p-channel) driven by a voltage between source and drain. The junction thus behaves like a field-effect transistor (FET).

The neuron-FET junction has certain features: (i) direct coupling of neuron and Si owing to an interaction of cell membrane and gate oxide without interfering metal; and (ii) well-defined structure and function made possible by the controlled attachment of an identified neuron to a microscopic transistor of matched design. These features can be compared to the characteristics of earlier approaches: A large (1 mm by 50 μm) FET with an open gate was used by Bergveld et al. to record extracellular voltage in muscle tissue (9). An FET with a metallized gate was used by Jobling et al. (10). An assembly of neuron and metallized Si was described by Regehr et al. (11).

Retzius cells (diameter about 60 μm) were isolated from segmental ganglia of the leech Hirudo medicinalis. The soma of the neuron together with a short neurite was dissociated after enzymatic treatment of opened ganglia (12, 13). In freshly dissociated cells the amplitude of the action potentials was 40 to 60 mV. Planar technology was used to fabricate p-channel insulated-gate FETs (14, 15). Source and drain were made on the (100) surface of n-Si by boron diffusion. The length of the channel between source and drain was 6 μm. Its width was 30 μm (Fig. 2). The channel region was insulated by a gate oxide 20 nm thick. A Perspex chamber was fixed on the Si plate (16). After the gate had been coated with poly-L-lysine, we filled the chamber with electrolyte (leech Ringer, pH 7.4). A neuron was attached on the tip of a glass pipette and mounted on the gate under visual control (Fig. 2) (17).

We performed four types of measurement (18) with the junctions (Fig. 3). (i) A single action potential was stimulated by current
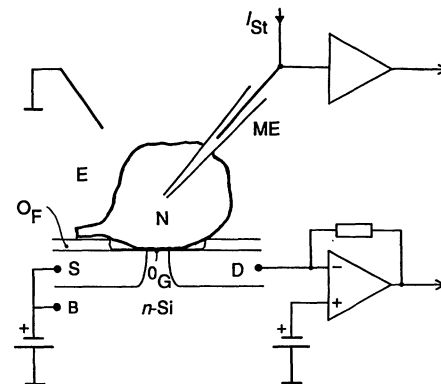

Fig. 1. Neuron-Si junction (unscaled). A neuron (N) is attached to oxidized Si. A thin layer of gate oxide (O_G, marked by the heavy line) covers n-type Si between the source (S) and drain (D) of p-type Si insulated by a thick field oxide (O_F). The electrolyte (E) is maintained at ground potential (Ag/AgCl electrode). Bulk silicon (B), source, and drain are held at positive bias voltages (p-channel FET). The source-drain current is measured by a current-voltage converter. The neuron is impaled by a microelectrode (ME) (Ag/AgCl). Current (I_{St}) is injected to stimulate the cell. The membrane potential is measured by a voltage follower.

Abteilung Biophysik der Universität Ulm, D-7900 Ulm-Eselsberg, Germany.

*To whom correspondence should be addressed.

injection through an impaled microelectrode. The change of intracellular voltage V_M (membrane potential) was up to 40 mV. The source-drain current I_D was lowered and was well correlated with the increase of V_M (Fig. 3A). The maximal change of current corresponded to the effect of a calibration voltage on the gate of $V_G = 9$ mV (compare the current-voltage relation of the FET in Fig. 3E). (ii) Using current pulses, we stimulated repetitive firing with a perfect match of I_D and V_M (Fig. 3B). (iii) We observed modulations of I_D without impaled microelectrode (Fig. 3C). The shape and amplitude of the response resembled the signals obtained by stimulation. (iv) Frequently we found modulations that resembled the first derivative of an action potential (Fig. 3D).

We prepared 54 neuron-Si contacts, and in most cases we studied each one for about 20 min. In eight samples we found a strong coupling of action potentials with an effective gate voltage of about 10 mV. In two of these contacts V_M was checked with a microelectrode. In six samples we observed a weak coupling of spikes with the shape of derivatives (amplitudes around 2 mV). In two of these contacts the shape changed occasionally such that it resembled the spike itself. In 14 samples we observed a very weak coupling of action potentials (<1 mV). In 15 samples we found a strong coupling of depolarizations as induced by current injection without triggering a spike. In 11 samples we could not detect any coupling. In two of these contacts action potentials were recorded by a microelectrode.

Apparently there are two problems: variable strength of coupling and variable activity of the neurons themselves. The variable coupling may be caused by a variable contact area of membrane and gate and by a variable cleft width between membrane and gate. The neurons may be damaged by the isolation, by manipulations in the procedure of attachment, by a toxic effect of poly-L-lysine, and by the impalement of the microelectrode. The FETs themselves were sufficiently stable. Within the first few hours in Ringer solution, their threshold (Fig. 3E) drifted by about 0.5 V. No change was observed, however, within 60 hours of further use. We assign the satisfactory stability to the positive polarization of n-Si, which repels sodium ions from the Si-SiO$_2$ interface. It may be optimized by depositing silicon nitride on the gate. The noise of I_D (Fig. 3) may be reduced by improved bond-

Fig. 2. Structure of the neuron-Si junction. (**A**) Top view of the FET with a Retzius cell. The horizontal band (width, 50 μm) reflects source and drain. (**B**) Top view of the FET. The visible distance between source and drain is 16 μm. The contours mark the range of primary deposition of boron (groove of depth 150 nm), not the location of the pn junctions. In the center the insulating oxide (1 μm) is opened over an area 22 μm by 30 μm. This region is covered by the gate oxide (thickness 20 nm). (**C**) The pn junctions. The lower half of the FET is ground at an angle of 2° up to the edge marked by the two arrows. The geometry is illustrated at the right (not scaled). The stripes are interference fringes due to the field oxide. The two pn junctions of source and drain—as stained by copper—are marked by arrows. Their horizontal distance at the gate is 6 μm.
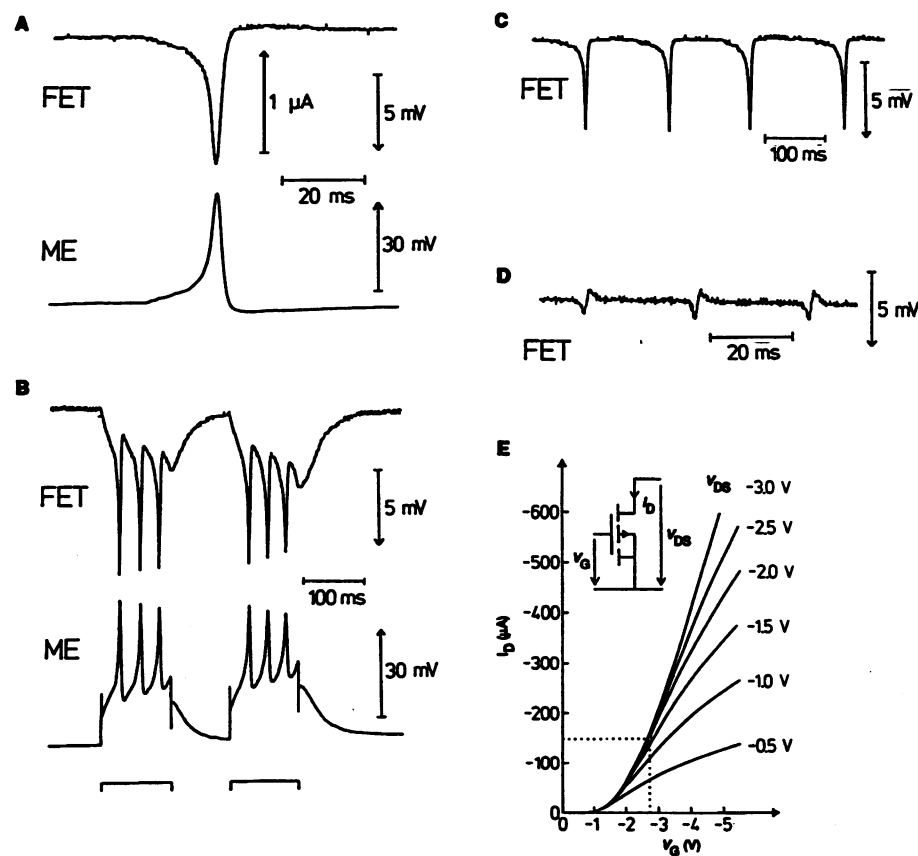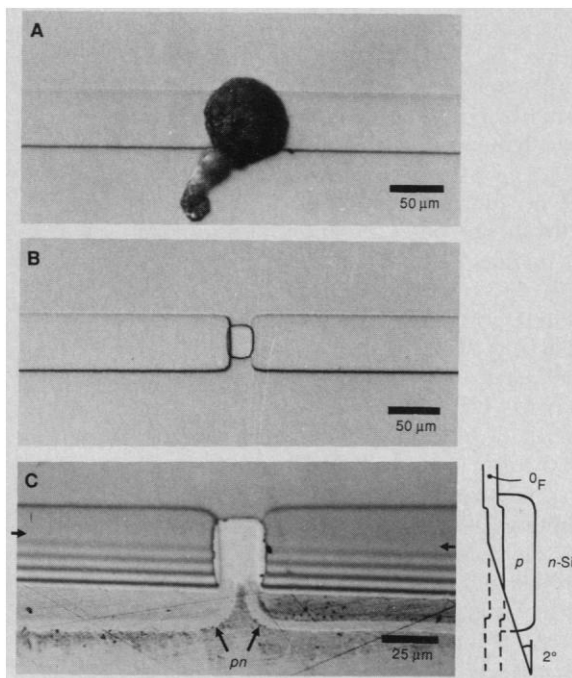

Fig. 3. Electrical junction of the Retzius cell and the FET: (**A**) Single action potential. The source-drain current I_D of the FET and the membrane potential V_M, as measured by an impaled microelectrode (ME), are shown. The effective gate voltage V_G is determined by calibration before attachment of the neuron [see the current-voltage relation in (E)]. The noise of the current is due to imperfections of FET fabrication. (**B**) I_D and V_M of a sequence of action potentials triggered by current pulses as marked at the bottom. The discontinuities in the trace of the V_M are due to the voltage drop of injection current in the microelectrode (unbalanced bridge). (**C**) I_D without impaled electrode. The signals resemble action potentials. (**D**) I_D without impaled electrode. The signals resemble first derivatives of action potentials. (**E**) Current-voltage characteristic of the FET in Ringer at pH 7.4. I_D versus V_G for various source-drain voltages V_{DS}.

ing and suppression of surface states.

To rationalize the junction, let us consider a minimal circuit of capacitive coupling as depicted in Fig. 4A. It consists of the capacitances C_{JM} and C_{JG} of membrane and gate and of the resistance R_J of the cleft. It is driven by the voltage V_M across the membrane capacitance C_M. The time course of the voltage $V_J(t)$ across C_{JG} is determined by Eq. 1. In the case of high seal resistance R_J, we expect proportionality of output and
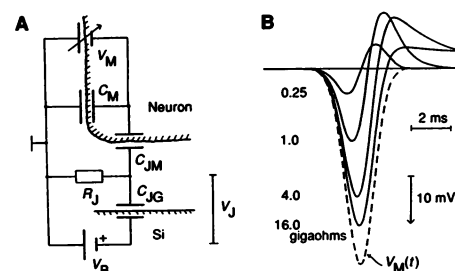

Fig. 4. Circuit of the neuron-Si junction. (**A**) The circuit consists of the capacitances C_{JM} and C_{JG}, characterizing the plasma membrane and the gate oxide in the junction, and of the resistance R_J characterizing the cleft between membrane and gate. The Si is kept at a voltage V_B. A variable voltage V_M (action potential) is applied across the capacitance C_M of the plasma membrane. The voltage V_J is detected by the source-drain current. (**B**) Simulation: A pulse $V_M(t)$ of Gaussian shape (amplitude, 40 mV; half width, 2 ms) is applied (dashed line). The voltage $V_J(t)$ is plotted for a junction with $C_{JM} = 0.6$ pF, $C_{JG} = 0.1$ pF, and $R_J = 0.25, 1, 4$, and 16 gigaohms. In the case of high resistance, the signal is transmitted efficiently at invariant shape; in the case of low resistance, the signal is differentiated and damped.
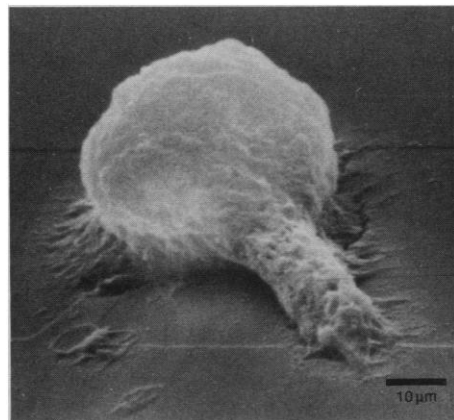

Fig. 5. Scanning electron micrograph of a Retzius cell on an FET. The contours of source and drain (region of primary deposition of boron, not *pn*-junctions) are visible. The distance of the contours of source and drain is 6 μm in this sample. The neuron is attached to Si by poly-L-lysine. It spreads on the coated Si such that an intimate contact of membrane and gate is formed. The assembly was fixed by glutardialdehyde 30 min after attachment of the neuron on the chip, that is, under the conditions used for electrical records. It was dehydrated in a series of water-propanol mixtures and dried. This procedure of fixation and dehydration shrinks the cell body by about 30%.

input as $V_J = V_M C_{JM}/(C_{JM} + C_{JG})$. In the case of low resistance the output resembles the damped derivative of the input as $V_J = R_J C_{JM} dV_M/dt$:

$$\frac{dV_J}{dt} = \frac{C_{JM}}{C_{JM} + C_{JG}} \frac{dV_M}{dt} - \frac{1}{R_J(C_{JM} + C_{JG})}V_J \tag{1}$$

We assign the large signals of perfect shape (Fig. 3, A through C) to tight capacitive coupling and the low signals of biphasic shape (Fig. 3D) to a low seal resistance. In a tight junction we expect $V_J/V_M = C_{JM}/(C_{JM} + C_{JG}) = 0.86$ (specific capacitances 1 μF per square centimeter of membrane and 0.16 μF per square centimeter of gate oxide of thickness 20 nm and dielectric constant 3.9). We observe a ratio $V_G/V_M = 0.25$ with respect to the effective gate voltage V_G (Fig. 3A). We assign the discrepancy of V_G and V_J to an incomplete gate-membrane contact. We may assume that the junction voltage V_J is effective only along a width w_J of the gate, whereas the calibration voltage V_G modulates I_D along the whole gate of width $w_G = 30$ μm. The effects of V_J and V_G are then identical per definition as expressed by $w_J V_J = w_G V_G$. Within this model the ratio $V_G/V_J = 0.3$ reflects the ratio w_J/w_G, that is, the junction covers 10 μm of the gate. We evaluate $V_J(t)$ for such a junction of area 6 μm by 10 μm according to Eq. 1 with $C_{JM}/(C_{JM} + C_{JG}) = 0.86$, $C_{JM} + C_{JG} = 0.7$ pF, and $R_J = 0.25, 1, 4$, and 16 gigaohms. A match of the pulse shapes of input and output is attained for high resistances $R_J > 10$ gigaohms (Fig. 4B). For low resistance the output resembles the derivative of the input at a reduced amplitude.

Apparently a tight seal of membrane and gate is the prerequisite for efficient coupling. As a first step toward a structural analysis of the junction, we looked at samples fixed with glutardialdehyde using a scanning electron microscope. The neuron spreads over the Si (Fig. 5). An intimate local contact between membrane and gate is likely.

The neuron-Si junction outdoes metallic microelectrodes where the amplitude of the extracellular voltage is in the range of 0.1 mV (*3–6, 8*) up to 1 mV (*10, 11*). We assign the good performance to the nature of capacitive coupling at high seal resistance as attained by tight adhesion of neuron and gate oxide without metallic conductor.

Owing to the simple geometry, no major problems should arise in the construction of patterns of FETs with gates of 10 μm on a single chip. Thus, multiple recording in cell cultures appears to be a feasible technique that may be applied to neurons in a network or to sites in a neuronal arborization. FET probes may be superior to impaled elec-

trodes and voltage-sensitive dyes, which interfere with cell activity. Long-term recordings at high resolution and high signal-to-noise ratios with these neuron-Si junctions may be possible.

REFERENCES AND NOTES

1. B. M. Salzberg, H. V. Davila, L. B. Cohen, *Nature* **246**, 508 (1973).
2. T. D. Parsons, D. Kleinfeld, F. Raccuia-Behling, B. M. Salzberg, *Biophys J.* **56**, 213 (1989).
3. G. W. Gross, E. Rieske, G. W. Kreutzberg, A. Meyer, *Neurosci. Lett.* **6**, 101 (1977).
4. J. Pine, *J. Neurosci. Methods* **2**, 19 (1980).
5. M. Kuperstein and H. Eichenbaum, *Neuroscience* **15**, 703 (1985).
6. J. L. Novak and B. C. Wheeler, *IEEE Trans. Biomed. Eng.* **33**, 196 (1986).
7. K. Takahasi and T. Matsuo, *Sensors Actuators* **5**, 89 (1984).
8. K. L. Drake, K. D. Wise, J. Farraye, D. J. Anderson, S. L. Bement, *IEEE Trans. Biomed. Eng.* **35**, 719 (1988).
9. P. Bergveld, J. Wiersma, H. Meertens, *ibid.* **23**, 136 (1976).
10. D. T. Jobling, J. G. Smith, H. V. Wheal, *Med. Biol. Eng. Comput.* **19**, 553 (1981).
11. W. G. Regehr, J. Pine, D. B. Rutledge, *IEEE Trans. Biomed. Eng.* **35**, 1023 (1988).
12. I. D. Dietzel, P. Drapeau, J. G. Nicholls, *J. Physiol. (London)* **372**, 191 (1986).
13. Segmental ganglia of *Hirudo medicinalis* (Biopharm, Swansea) were dissected and pinned on a dish coated with Sylgard (Dow-Corning) in L-15 medium (Gibco, Eggenstein) [supplemented with 2% fetal calf serum, glucose (6 mg/ml), and gentamycin sulfate (50 μg/ml)]. The capsules were opened and incubated at room temperature for 1 hour with dispase-collagenase (Boehringer Mannheim) at a concentration of 2 mg/ml. The Retzius cells were dissociated by aspiration into a fire-polished micropipette and washed with several drops of supplemented medium and kept in the medium for 4 to 6 hours such that the cells lost most of remaining connective tissue. Then they were transferred into leech Ringer.
14. S. Wolf and R. N. Tauber, *Silicon Processing for VLSI Era* (Lattice Press, Sunset Beach, CA, 1986).
15. Samples were cut from *n*-type Czochralski-Si wafers [(100) surface, 5 to 10 ohm-cm] (Wacker-Chemie, Burghausen) at a size of 30 mm by 10 mm. On every plate six FETs were fabricated at a spacing of 2 mm. The plates were cleaned according to the procedure of the RCA (Radio Corporation of America), and silicon oxide was grown in wet O_2 at 1000°C. A mask of positive photoresist (AZ-1514, Hoechst, Frankfurt) was prepared. The source and drain regions (distance, 16 μm) were opened by ammonium fluoride solution (AF 87.5-12.5, Merck, Darmstadt). A boron glass was deposited by evaporation from planar sources of boron nitride (Sohio Engineered Materials Company, New York) at 900°C. The boron was driven in at 1120°C for 7 hours. Boron glass and silicon oxide were removed and a layer of oxide (1 μm) was grown at 1100°C. The gate was reopened (area, 22 μm by 30 μm) and a thin layer of oxide (20 nm) was grown in dry O_2 at 1000°C. The thickness of the oxide layers was evaluated from angle-dependent light reflection. After reopening the contact sites on source, drain, and bulk Si, we applied Al contacts by using evaporation and the lift-off technique. The chip was annealed at 350°C for 5 min. We checked the profile of the FET by grinding at an angle of 2° and staining the *pn*-junction. The depth of the *pn*-junction was 5 μm. The distance between the *pn*-junctions in the gate was 6 μm.
16. The chamber was a wedge-shaped slot with width at the top 8 mm, width at the bottom 2 mm, length at the bottom 12 mm, in a piece of Perspex (thickness, 10 mm). We attached the Perspex to the Si plate using Sylgard such that the contact sites of source and drain stuck out beyond the Perspex.
17. The Si surface was cleaned with hot basic hydrogen peroxide as used in RCA cleaning (30% hydrogen

peroxide:25% ammonia:water = 1:1:5, 80°C). A drop of poly-L-lysine (molecular weight 15,000 to 30,000, Sigma, Heidelberg) at a concentration of 1 mg/ml in water was applied to the gate and dried. The chamber was filled with leech Ringer (115 mM NaCl, 4 mM KCl, 1.8 mM CaCl$_2$, 10 mM tris-maleate, pH 7.4). A neuron was sucked several times into a wide glass pipette (tip diameter, 80 to 100 μm) to remove connective tissue and was transferred into the chamber. We attached the cell to a narrow pipette (tip diameter, 10 to 25 μm) by suction and pressed it gently onto the gate with a micromanipulator and a stereomicroscope. The micropipette was removed. The attachment was completed within a few minutes after addition of Ringer to the chamber as the coat of poly-L-lysine faded away. Measurements with the FET were started within a minute after attachment. After tests to record spontaneous activity, we impaled a microelectrode (tip diameter <1 μm). After completion of the measurements, the chip was cleaned with water and hot basic hydrogen peroxide and reused.

18. Bulk Si and source were kept at 2.7 V and the drain was kept at 0.7 V such that the source-drain voltage V$_{DS}$ was −2 V as marked in Fig. 3E. The current was fed into a current-voltage converter. After amplification and filtering, the signal was digitized and read into a computer. All measurements were performed in the dark to avoid photocurrents. The neuron was impaled by a glass microelectrode filled with 3 M KCl and contacted with a Ag/AgCl electrode. It was connected to a voltage follower of standard design such that the membrane potential was measured at low impedance and current could be injected through the electrode. The signal was digitized and read into the computer.

Spectroscopic Observations of Bright and Dark Emission Features on the Night Side of Venus

J. F. BELL III,* D. CRISP, P. G. LUCEY, T. A. OZOROSKI, W. M. SINTON, S. C. WILLIS, B. A. CAMPBELL

Near-infrared spectra of a bright and a dark thermal emission feature on the night side of Venus have been obtained from 2.2 to 2.5 micrometers (μm) at a spectral resolution of 1200 to 1500. Both bright and dark features show numerous weak absorption bands produced by CO$_2$, CO, water vapor, and other gases. The bright feature (hot spot) emits more radiation than the dark feature (cold spot) throughout this spectral region, but the largest contrasts occur between 2.21 and 2.32 μm, where H$_2$SO$_4$ clouds and a weak CO$_2$ band provide the only known sources of extinction. The contrast decreases by 55 to 65 percent at wavelengths longer than 2.34 μm, where CO, clouds, and water vapor also absorb and scatter upwelling radiation. This contrast reduction may provide direct spectroscopic evidence for horizontal variations in the water vapor concentrations in the Venus atmosphere at levels below the cloud tops.

NEAR-INFRARED (NIR) IMAGES and spectra of Venus acquired by Allen and Crawford (1) revealed that the night side of the planet was unexpectedly bright at wavelengths near 1.7 and 2.3 μm, in atmospheric windows between strong CO$_2$ and water vapor absorption bands. These authors concluded that this night-side radiation was produced thermally in the hot lower atmosphere of Venus. The bright-contrast and dark-contrast features were thought to be produced as this radiation passes through a higher, cooler, optically thin cloud region. Subsequent observations and theoretical analysis confirmed these conclusions. Allen (2) ratioed low-resolution spectra of bright and dark regions of the Venus night side and found that this ratio was almost independent of wavelength. This result implies that the agent that produces the dark features is a continuum absorber, such as the H$_2$SO$_4$ cloud droplets, rather than a gas. Kamp et al. (3) showed that the night side radiation could be completely accounted for by thermal emission from the pressure-broadened far wings of CO$_2$ and H$_2$O lines in the deep Venus atmosphere. Their results also showed that intensity contrasts as large as those observed on the night side could be produced by variations in the cloud optical depth of 20%. Crisp et al. (4) combined infrared images of Venus with Allen's spectra and spacecraft observations (5) and showed that the features were produced by horizontal variations in the optical depth of the middle or lower cloud deck at altitudes between 48 and 55 km. The feature rotation period at those levels was found to be about 6 ± 1 days, indicating equatorial east-west

J. F. Bell III, P. G. Lucey, T. A. Ozoroski, B. A. Campbell, Planetary Geosciences Division, University of Hawaii, Honolulu,HI 96822 and Visiting Astronomers at the Infrared Telescope Facility, operated by the University of Hawaii under contract to the National Aeronautics and Space Administration.
D. Crisp, Jet Propulsion Laboratory and California Institute of Technology, Mail Stop 169-237, 4800 Oak Grove Drive, Pasadena, CA 91109.
W. M. Sinton, Institute for Astronomy, University of Hawaii, Honolulu, HI 96822.
S. C. Willis, Remote Sensing Lab, Mail Stop AJ-20, University of Washington, Seattle, WA 98195.

*To whom correspondence should be addressed.

wind velocities of about 70 m/s. Bezard et al. (6) analyzed new high-resolution spectra of a bright region on the Venus night side and showed that the thermal emission in the 2.3-μm region originates primarily at levels above 8 bars (30 km), whereas the 1.74-μm radiation is produced at deeper levels. Their spectra placed new constraints on the concentrations of several important trace gases in the lower Venus atmosphere, including H$_2$O, CO, HCL, and HF. They also provided an independent confirmation of the enhanced D/H ratios observed by Pioneer Venus (7) and provided the first true detection of OCS in the Venus atmosphere.

New imaging and spectroscopic observations of the Venus night side were taken from a global network of observatories during January and February of 1990 to support the Galileo spacecraft Venus flyby. On 10 February 1990 UT the Galileo Near-Infrared Mapping Spectrometer (NIMS) was the first spacecraft instrument to take NIR images and spectra of the Venus night side. These data have better spatial resolution than the ground-based data, but severe limits on the data telemetry rate and on spacecraft tape recorder storage restricted the spatial, temporal, and spectral coverage of the NIR features.

To complement the Galileo NIMS experiment we conducted daytime spectroscopic observations of Venus from the National Aeronautics and Space Administration (NASA) Infrared Telescope Facility (IRTF) at Mauna Kea Observatory during 26 to 30 January 1990. This observing period was ideal for spatially resolved studies of the night side of Venus because passage of the planet through inferior conjunction less than 2 weeks before provided a relatively large disk (60 arc seconds) and a thin sunlit crescent (α = 155°). We used the Cooled-Grating Array Spectrometer (CGAS) to provide a spectral resolution between 1200 and 1500 in the 1.7- and 2.3-μm windows (8). The CGAS has a 2.7-arc second circular entrance aperture and yielded an effective spatial resolution of 550 km on the Venus night side. Because Venus was perilously close to the sun in the morning sky, we used a special telescope mask to prevent sunlight from striking the primary mirror (9).

We coordinated our spectroscopic observation program with a concurrent NIR imaging program lead by Sinton and co-workers at the University of Hawaii Air Force 61-cm telescope on Mauna Kea (10). Their images allowed us to acquire spectra of the darkest and brightest features on the Venus night side. A 2.36-μm NIR camera image acquired on the morning of 29 January 1990 UT showed a large (~5-arc second) hot spot on the Venus night side centered at